Published in final edited form as:
J Bone Miner Res. 2012 November ; 27(11): 2359–2372. doi:10.1002/jbmr.1687.

Connexin 43 Deficiency Attenuates Loss of Trabecular Bone and Prevents Suppression of Cortical Bone Formation During Unloading

Shane A. Lloyd, B.S., **Gregory S. Lewis, Ph.D.**, **Yue Zhang, Ph.D.**, **Emmanuel M. Paul, B.S.**, and **Henry J. Donahue, Ph.D.**
Division of Musculoskeletal Sciences, Department of Orthopaedics and Rehabilitation, Penn State College of Medicine, 500 University Drive, Hershey, PA 17033

Abstract

Connexin 43 (Cx43) is the most abundant gap junction protein in bone and has been demonstrated as an integral component of skeletal homeostasis. In the present study, we sought to further refine the role of Cx43 in the response to mechanical unloading by subjecting skeletally mature mice with a bone-specific deletion of Cx43 (cKO) to three weeks of mechanical unloading via hindlimb suspension (HLS). The HLS model was selected to recapitulate the effects of skeletal unloading due to prolonged bed rest, reduced activity associated with aging, and spaceflight microgravity. At baseline, the cortical bone of cKO mice displayed an osteopenic phenotype, with expanded cortices, decreased cortical thickness, decreased bone mineral density, and increased porosity. There was no baseline trabecular phenotype. Following three weeks of HLS, wild-type (WT) mice experienced substantial declines in trabecular bone volume fraction, connectivity density, trabecular thickness, and trabecular tissue mineral density. These deleterious effects were attenuated in cKO mice. Conversely, there was a similar and significant amount of cortical bone loss in both WT and cKO. Interestingly, mechanical testing revealed a greater loss of strength and rigidity for cKO during HLS. Analysis of double-label quantitative histomorphometry data demonstrated a substantial decrease in bone formation rate, mineralizing surface, and mineral apposition rate at both the periosteal and endocortical surfaces of the femur following unloading of WT mice. This suppression of bone formation was not observed in cKO mice, where parameters were maintained at baseline levels. Taken together, the results of the present study indicate that Cx43 deficiency desensitizes bone to the effects of mechanical unloading, and that this may be due to an inability of mechanosensing osteocytes to effectively communicate the unloading state to osteoblasts to suppress bone formation. Cx43 may represent a novel therapeutic target for investigation as a countermeasure for age-related and unloading-induced bone loss.

Keywords

connexin 43; unloading; hindlimb suspension; gap junction; bone loss

CORRESPONDING AUTHOR: Henry J. Donahue, Ph.D., Division of Musculoskeletal Sciences, Department of Orthopaedics and Rehabilitation, Penn State College of Medicine, 500 University Drive, Hershey, PA 17033, Telephone: 717-531-4819, Fax: 717-531-7583, hdonahue@psu.edu.
Authors roles: Study design: SAL, YZ, EMP, HJD; Study conduct: SAL, YZ, EMP; Data collection: SAL, YZ, EMP; Data interpretation: SAL, GSL, EMP, HJD; Drafting manuscript: SAL, GSL, HJD; Revising manuscript content: SAL, GSL, HJD; Approving final version of manuscript: SAL, HJD. SAL takes responsibility for the integrity of the data analysis.

DISCLOSURES
The authors have no financial interests or conflicts of interest to disclose.

INTRODUCTION

Gap junctions (GJs) are membrane-spanning protein channels that allow for the passage of small molecules between adjacent cells (1), or when unopposed as hemichannels, between the cell and extracellular environment (2). Bone cells have been shown to primarily express the GJ protein connexin 43 (Cx43) (3). Studies from our laboratory and others have demonstrated that Cx43 expression and gap junctional intercellular communication (GJIC) play a critical role in the differentiation and activity of osteoblasts (4), osteoclasts (5), and osteocytes (6). Aside from its role in transmitting small molecules, Cx43 has also been shown to interact with various signaling molecules and structural proteins required for osteoblast and osteocyte function (2,7-9). Cx43 also plays an integral role in skeletal development, as evidenced by oculodentodigital dysplasia, a rare genetic disorder manifested in individuals with mutations in the Cx43 gene (*Gja1*) (10).

Numerous studies have demonstrated a critical role of Cx43 in the skeletal response to mechanosensing both *in vitro* (11,12) and *in vivo* (13,14). Indeed, we recently published findings of an enhanced anabolic response of Cx43-deficient mice following an *in vivo* mechanical loading regimen (14). However, only one study has focused on the role of Cx43 in response to unloading (15). Practical examples of mechanical unloading include that experienced during periods of bed rest due to neurological injury or trauma (16), in the elderly due to reduced physical activity (17), or in astronauts exposed to the “weightless” environment of spaceflight (18). Studies of prolonged head down bed rest have demonstrated significant loss of bone mineral density (BMD) and cortical bone mass (19,20). During missions on the International Space Station, astronauts have been found to experience bone loss on the order of 1% per month in load bearing bones (21). Surprisingly, even a year after return to Earth, astronaut BMD had not fully recovered (22). Bone loss due to unloading, whether due to spaceflight or clinically relevant scenarios, may increase fracture risk and increase individual morbidity and mortality (23,24).

In the present study, we have employed the well-validated, ground-based model of unloading called hindlimb suspension (HLS). The HLS technique was developed by Morey-Holton and colleagues at the National Aeronautics and Space Administration (NASA) Ames Research Center (25). This model has been extensively validated in the literature and is able to recapitulate the primary aspects of microgravity and bed rest unloading, including a lack of weight bearing in the hind quarters and a cephalic fluid shift (26). A previous study by Grimston and colleagues utilized a botox model of muscle paralysis and found attenuated cortical bone loss in Cx43 deficient mice (15). However, the unique aspects of the HLS model will allow us to further refine the role of Cx43 in the skeletal response to mechanical unloading.

We investigated the response of skeletally mature mice with a bone-specific deletion of Cx43 to three weeks of HLS. Suspension resulted in substantial degradation of trabecular bone, an effect that was significantly attenuated in cKO mice. In the cortical bone compartment, Cx43 deficiency prevented unloading-induced suppression of bone formation. Our results indicate that Cx43 deficiency is protective against unloading induced bone loss, particularly in the trabecular bone compartment, and may represent a potential therapeutic target for the prevention of unloading-induced bone loss.

METHODS

Transgenic mice

Our strategy for generation of transgenic mice, confirmation of conditional knockout in osteocytes/osteoblasts, and determination of the specificity of the Cx43 deletion was

described previously (14). Briefly, mice expressing Cre recombinase under the control of the human osteocalcin promoter (OC-Cre; $Cx43^{+/+}$) (27) were bred with mice in which the Cx43 gene (*Gja1*) is flanked by two loxP sites ($Cx43^{flx/flx}$) (28) to generate OC-Cre; $Cx43^{flx/+}$ mice. We then crossed OC-Cre; $Cx43^{flx/+}$ mice with $Cx43^{flx/flx}$ mice to generate OC-Cre; $Cx43^{flx/flx}$ mice. We then back bred OC-Cre; $Cx43^{flx/flx}$ mice with $Cx43^{flx/flx}$ mice to generate an equal number of OC-Cre; $Cx43^{flx/flx}$ (conditional C43 deficient equivalent; cKO) and $Cx43^{flx/flx}$ (wild-type; WT). Mice derived from this breeding strategy were bred with C57BL/6 mice for three generations, resulting in mice with a C57BL/6 background. Genotyping was performed by polymerase chain reaction techniques using genomic DNA isolated from mouse earpieces and primers as described previously (14).

Animal Procedures

The present study utilized skeletally mature, six-month-old male Cx43 cKO and WT mice. Mice were housed in the central animal facility at the Penn State College of Medicine (Hershey, PA, USA). Mice were fed standard laboratory rodent chow, maintained at a constant temperature of 25°C, and kept on a 12 hour light/dark cycle during all experimental procedures. Mice were housed in standard vivarium enclosures until one-week prior to experimentation, when they were moved to the hindlimb suspension (HLS) enclosures (2 mice per cage) in order to acclimatize under normal loading conditions. WT and cKO mice were then divided into normally loaded (i.e., Control) and HLS (i.e., Suspended) groups (n=10-15/group). The experimental period of unloading was three weeks. This time frame was selected based on a preliminary study (data not shown) demonstrating significant loss of both trabecular (~60%) and cortical bone (~15%) in WT mice. This degree of bone loss would allow us to effectively quantify potentially attenuated bone loss in cKO mice, while still allowing for additional loss in the event that Cx43 deficiency exacerbated unloading-induced bone loss.

The HLS method utilized was a modified version of that first described by Morey-Holton and colleagues (25). Mice were suspended at a 30° elevation. This angle has been previously demonstrated to keep the forelimbs normally-loaded, while minimizing tail tension and animal stress (29). The forelimbs of the animal remained on the wire mesh cage bottom, allowing the animal free access to food and water. Two mice were suspended per cage, although their placement at opposite ends prevented physical contact. Control mice were housed in this same cage environment. The health and activity of the animals was assessed daily throughout the experiment by laboratory and veterinary staff. Mice were detached from the HLS enclosure and placed in a container with an overhead crossbar that allowed for measurement of animal mass without reloading. All animal procedures were approved by the Institutional Animal Care and Use Committee at the Penn State College of Medicine (Protocol 2010-117).

In Vivo MicroComputed Tomography

In vivo scans of trabecular and cortical microarchitecture were conducted using a Scanco vivaCT 40 (Scanco Medical AG, Brüttisellen Switzerland). Scans were conducted immediately prior to the start of the study (baseline; day 0) and at the study endpoint (day 21). The right hindlimb of each animal was extended and held in a reproducible position using a rodent hindlimb immobilization device provided by Scanco Medical AG. The snout of the animal was placed in a cone in order to maintain it under anesthesia (2% isoflurane) during the 28 minute scanning procedure. Trabecular microarchitecture was quantified based on a 72 slice region of the proximal tibia, immediately distal to the epiphyseal plate. Cortical parameters were quantified based on a 22 slice region of the femoral midshaft. These regions were scanned using settings of 55 KVp, 145 μA, and a 200 ms integration time. Images were reconstructed as a matrix of 2048×2048×76 isotropic voxels measuring 10.5

μm. Images were gaussian filtered (sigma = 1.5, support =2) and a threshold (27.5% of full scale) was applied to remove the surrounding soft tissue. The periosteal and endosteal boundaries of the cortical bone were segmented using the Scanco semi-automated edge detection algorithm. The region of interest in trabecular bone was manually segmented. Each mouse was scanned just twice (i.e., baseline and endpoint), thus limiting the potential effect of microCT-related radiation effects on bone structure (30).

Bone microarchitectural parameters were analyzed and reported as per previously published guidelines (31). Trabecular parameters included bone volume fraction (BV/TV; %), trabecular number (Tb.N; 1/mm), trabecular thickness (Tb.Th; mm); trabecular separation (Tb.Sp; mm), structure model index (SMI; no units), connectivity density (Conn.D; $1/mm^3$), and trabecular tissue mineral density (TMD; mg HA/cm^3). Cortical parameters included total cross-sectional area inside the periosteal envelope (Tt.Ar; mm^2), cortical bone area (Ct.Ar; mm^2) = cortical volume (Ct.V) ÷ (number of slices × slice thickness), cortical area fraction (Ct.Ar/Tt.Ar; %), marrow area (Ma.Ar; mm^2), average cortical thickness (Ct.Th; mm), cortical porosity (Ct.Po; %), cortical bone mineral density (BMD; mg HA/cm^3), and polar moment of inertia (pMOI; mm^4)

Biomechanical Testing

Right femurs, used for baseline and endpoint microCT scans, were isolated, cleaned of all non-osseous tissue and stored in phosphate-buffered saline (PBS) at −80°C. Bones were warmed to room temperature before being mechanically tested to failure via three-point bending using an MTS MiniBionix 858 testing apparatus (MTS Systems, Eden Prairie, MN, USA) (32). The flexural support spans were 8 mm, while a loading rate of 1 mm/minute was applied. Femurs were consistently oriented so the loading occurred in the medial to lateral direction.

Using the displacement (d) and force (F) data collected by the device during loading to fracture it was possible to calculate several parameters describing the whole-bone structural properties. Based on classical beam theory, force was converted to bending moment ($M = FL/4$), where L = span length of 8 mm. Displacement was normalized based on the span length ($d' = 12d/L^2$) as described previously (33,34). From the resulting plot of M versus d', ultimate bending moment, rigidity (slope of the linear portion of the curve), and ultimate energy (area under the curve) were computed.

Dynamic Histomorphometry

Immediately prior to suspension, mice were administered an intraperitoneal injection of Calcein (Sigma-Aldrich; St Louis, MO, USA) at 10 mg/kg body weight and 14 days later injected with Alizarin Red (Sigma-Aldrich) at 30 mg/kg body weight. Seven days after the second injection (Day 21, study endpoint) mice were sacrificed and the left femurs were dissected and embedded using an Osteo-Bed bone embedding kit (Polysciences, Warrington, PA, USA) following the manufacturer's protocol. The embedded femur midshafts were then cut into about 100 μm thick discs followed by abrasive polishing to a thickness of about 50 μm with lapping films (3M, St. Paul, MN, USA). Digital images were obtained using a confocal microscope (Leica, Bannockburn, IL, USA) at 4× under a UV light source with red and green filters. The following periosteal (Ps) and endcortical (Ec) bone parameters were quantified with ImageJ (NIH, Bethesda, MD, USA): total perimeter (B.Pm); single label perimeter (sL.Pm); double label perimeter (dL.Pm), and double label area (dL.Ar). The following values were then calculated at both the Ps and Ec surface: bone surface (BS; mm^2), mineralizing surface (MS/BS = [1/2sL.Pm + dL.Pm]/B.Pm x100; %); mineral apposition rate (MAR = dL.Ar/dL.Pm/14 days; μm/day) and bone formation rate (BFR/BS = MAR × MS/BS × 3.65; $\mu m^3/\mu m^2$ per year) (35). Also calculated were total tissue volume

(Tt.V; mm^3), marrow cavity volume (Ma.V; mm^3), and cortical bone volume (Ct.V = Tt.V − Ma.V; mm^3) (36).

Muscle Assays

Prior to harvest of the femur, the left and right gastrocnemius muscles were isolated and weighed separately using an analytical scale, and then averaged.

Nuclear Magnetic Resonance (NMR) Body Composition

In order to detect any phenotypic differences in the relative percentage of lean, fat, and fluid mass in WT versus cKO mice, body composition was determined noninvasively in conscious animals (n=16/genotype) using a ^{1}H-NMR analyzer (Bruker LF90 Proton-NMR Minispec: Bruker Optics, Woodlands, TX, USA) (37). Mice were individually loaded into a plastic tube and inserted into the device for the one-minute scanning period. Due to limitations in equipment availability, scans were conducted to assess baseline differences in body composition only.

Statistical Analyses

Statistical analysis was conducted using GraphPad Prism Version 5.0 (GraphPad Software Inc., La Jolla, CA, USA). Data are expressed as means ± SEM. Statistical significance was assessed by Student's t-test when comparing two groups. Two-way ANOVA was used to assess multiple group comparisons (percent change from baseline or absolute values) and a Bonferroni post-hoc test to assess differences between groups. For all comparisons, $p<0.05$ was considered significant, unless indicated otherwise. In figures or tables with multiple groups, different letters indicate a significant difference, while the same letters indicate no difference.

RESULTS

Animal body composition

Average baseline body mass of six-month-old, male Cx43 conditional knockout mice (cKO; 33.99±0.81 g) was not significantly different from wild-type (WT; 32.83±0.70 g) ($p>0.05$). Mice in both groups lost approximately 8% body mass following three weeks of HLS ($p<0.05$). Qualitative assessment of ambulation, food and water intake, and general body habitus suggested an initial 2-3 day period of adaptation with reduced feeding, although all parameters increased and stabilized thereafter. Assessment of baseline body composition via ^{1}H-NMR revealed no significant differences for WT versus cKO for percent fluid (7-8%), fat (10-11%), or lean tissue (70-71%) ($p>0.05$; Figure 1A). Following three weeks of HLS, mass of the hindlimb gastrocnemius muscle was 20% lower in both WT and cKO groups ($p<0.05$, Figure 1B).

Cx43 cKO mice have an osteopenic cortical phenotype

Cortical microstructure was assessed using microcomputed tomography (microCT) scans of the right femur at the mid-diaphysis. Consistent with our previous findings (14), cKO mice demonstrated an osteopenic cortical phenotype. When compared to WT, cKO mice had 26% greater cortical bone area (Ct.Ar; Figure 2A) ($p<0.001$). Combined with a 57% increase in total cross-sectional area within the periosteal envelope (Tt.Ar; Figure 2B) ($p<0.0001$), this resulted in a 20% lower cortical area fraction (Ct.Ar/Tt.Ar; Figure 2C) ($p<0.0001$) for cKO versus WT. Ma.Ar was correspondingly 77% greater in cKO (3.11±0.02 mm^2) versus WT (1.76±0.02 mm^2) ($p<0.0001$). Average cortical thickness (Ct.Th; Figure 2D) and cortical bone mineral density (BMD; Figure 2E) were also significantly lower for cKO mice versus WT ($p<0.05$ and $p<0.0001$, respectively). Cortical porosity (Ct.Po; Figure 2F) was 159%

greater in cKO mice versus WT ($p<0.01$). The significant expansion of the cortical envelope and degradation of cortical bone microstructure in cKO mice is highlighted in a representative 2D microCT image (Figure 2G). With respect to total femur length, there was no difference between WT (15.7±0.1 mm) and cKO (15.8±0.1 mm) ($p>0.05$).

Cx43 cKO mice have no trabecular phenotype

Trabecular parameters were assessed using microCT scans of the right proximal tibia, immediately distal to the epiphyseal plate. There were no significant differences between WT and cKO for any of the trabecular parameters that were assessed (Table 1).

Cx43 deficiency attenuates the loss of trabecular microstructure during unloading

Three weeks of unloading via HLS resulted in a dramatic deterioration of trabecular bone, an effect that was attenuated in cKO mice. Trabecular bone volume fraction (BV/TV) decreased 67% for WT mice following HLS, while cKO mice experienced a significantly lower 53% decline (Figure 3A; $p<0.01$). Similarly, trabecular connectivity density (Conn.D) decreased 64% for WT and just 50% for cKO mice (Figure 3B; $p<0.05$). Although the effect was more modest, trabecular TMD experienced a similar result: declining 3% in WT and just 1% in cKO (Figure 3C; $p<0.05$). Tb.Th declined 35% in WT mice subjected to HLS, while cKO experienced a smaller 21% decrease (Figure 3D; $p<0.001$). There were also similar statistical trends indicating attenuated increase in trabecular separation (Tb.Sp; $p=0.1$) and decrease in trabecular number (Tb.N; $p=0.15$) for cKO mice (Figure 3E,F). The deleterious effects of unloading on trabecular microstructure, as well as the attenuated response in cKO mice, can be seen in the representative 3D microCT reconstructions at baseline (Day 0) and following three weeks of HLS (Day 21) (Figure 4; left-side images).

Cx43 deficiency has no effect on loss of cortical microstructure during unloading

The effect of HLS on cortical bone was modest compared to findings in the trabecular compartment. There was also no difference in loss of cortical microstructure between WT and cKO for any of the parameters assessed by microCT techniques. There was no significant effect of HLS on Tt.Ar for either genotype (Figure 5B; $p>0.05$). The other cortical parameters assessed, including Ct.Ar, Ct.Ar/Tt.Ar, and Ct.Th all decreased by approximately 14% for both WT and cKO following three weeks of unloading (Figure 5A,C,D; $p>0.05$ for WT vs. cKO). During unloading, cortical Ma.Ar increased by a significant 9.1±1.1% for cKO and a similar 9.4±0.5% for WT ($p<0.05$), with no change for control animals of either genotype. There was a difference in cortical BMD between Control and Suspended animals in the WT group, which was not present in cKO (Figure 5E; $p>0.05$), although the change in cortical BMD for WT versus cKO mice subjected to unloading was not significantly different ($p>0.05$). Changes in Ct.Po were highly variable for all groups, resulting in no significant differences detected between WT and cKO (Figure 5F; $p>0.05$). There was no difference in femur length between WT and CKO for control or suspended mice (data not shown). The relatively modest effects of unloading on cortical microstructure can be seen in representative microCT reconstructions at baseline (Day 0) and following three weeks of HLS (Day 21) (Figure 4; right-side images).

Cx43 cKO mice have greater femur strength at baseline, but similar strength to WT following unloading

At baseline, Cx43 cKO mice had significantly greater geometric resistance to torsion, as highlighted by the 96% greater polar moment of inertia (pMOI) (Figure 6A $p<0.0001$). Mechanical testing of femurs via three-point bending at the study endpoint revealed that normally loaded, control cKO mice had 23% greater ultimate bending moment (i.e., whole-bone strength) and 24% greater ultimate bending energy than control WT mice (Figure

6C,E; $p<0.05$ for both). There was no difference in bending rigidity between control cKO and WT (Figure 6D; $p>0.05$).

Mechanical testing of femurs from mice subjected to HLS revealed a relatively greater decrease in strength in cKO compared to WT. Ultimate bending moment in unloaded cKO mice was 24% lower than control cKO, whereas the difference between unloaded and control for WT mice was 18% (Figure 6C). There were similar findings for bending rigidity (Figure 6D) and ultimate bending energy (Figure 6E), which saw relatively greater decreases in parameters for suspended versus control in cKO mice. There was a similar 13% decrease in pMOI for both WT and cKO mice subjected to unloading via HLS (Figure 6B, I; $p>0.05$).

Cx43 deficiency attenuates unloading-induced suppression of cortical bone formation

Cortical morphological parameters as assessed via quantitative histomorphometry techniques (Table 2) followed a similar pattern as those acquired via microCT techniques at baseline (Figure 2). cKO mice had expanded cortices as indicated by the significantly greater total tissue volume (Tt.V), cortical bone volume (Ct.V), and marrow cavity volume (Ma.V) for control cKO versus control WT ($p<0.05$). There was also correspondingly greater endocortical bone surface (Ec.BS) and periosteal bone surface (Ps.BS) for control cKO versus control WT ($p<0.05$).

The reduced resolution and increased variability in measurement with this methodology, however, prevented resolution of the modest changes that occurred to cortical bone parameters during unloading as detected by microCT (i.e., 10-15% changes in Ct.Ar, Ct.Ar/Tt.Ar, and Ct.Th in Figure 5). As a result, there were no detected differences in these parameters between control and suspended for either genotype, although there were trends suggesting a reduction for Ct.Ar.

With regards to normally loaded control animals, there was no significant difference between WT and cKO at the endocortical surface with respect to mineralizing surface normalized to bone surface (MS/BS; Figure 7A), mineral apposition rate (MAR; Figure 7B), or bone formation rate normalized to bone surface (BFR/BS) (Figure 7C) ($p>0.05$ for all). Conversely, at the periosteal surface, MAR of cKO mice was 43% lower than WT (Figure 7B; $p<0.05$) and BFR/BS was 33% lower than WT (Figure 7C; $p<0.05$). There was no difference in Ps.MS/BS between WT and cKO (Figure 7A; $p>0.05$).

Unloading resulted in significant suppression of bone formation in WT mice, an effect that was not observed in cKO. This is illustrated rather vividly by representative black-and-white micrographs (Figure 7G), which demonstrate prominent incorporation of Calcein and alizarin red bone labels (white areas indicated by solid arrows at the periosteal surface and hatched arrows at the endocortical surface) in control WT animals, but not in suspended WT. Similar levels of incorporation are observed in both control and suspended cKO mice, indicating preservation of bone formation during unloading.

At the endocortical surface in WT mice, bone formation was essentially obliterated following three weeks of unloading. MS/BS of WT suspended animals was 75% lower than WT control (Figure 7B; $p<0.05$), while Ec.MAR and Ec.BFR/BS were reduced to zero due to the lack of any observed double labels. Conversely, there were no significant differences between control and suspended cKO mice with respect to Ec.MS/BS, Ec.MAR, or Ec.BFR (Figure 7A,B,C; $p>0.05$). The effects of unloading at the periosteal surface were more modest, although a similar trend was apparent. In WT mice subjected to unloading, Ps.MS/BS was 38% lower than WT control (Figure 7D; $p<0.05$). Ps.MS/BS was 41% lower in WT suspended versus control (Figure 7E; $p<0.05$), while Ps.BFR was 60% lower (Figure 7F; $p<0.05$). Similar to findings at the endocortical surface, these parameters were not

significantly different between suspended and control for cKO mice (Figure 7D,E,F; $p>0.05$).

DISCUSSION

Mechanical unloading via HLS results in dramatic deterioration of trabecular bone microstructure as well as suppression of periosteal and endocortical cortical bone formation in WT mice. These effects were significantly attenuated in mice with conditional knockout of the Cx43 gene *Gjal*. The effects of unloading on cortical bone microstructure were modest, with no detected difference in cortical bone loss between genotypes. At baseline, femurs from skeletally mature cKO mice have greater mechanical strength but similar rigidity compared to WT; however, they tended to lose a greater proportion of these parameters during unloading. Taken together, these results indicate that a deficiency of Cx43 in osteocytes and osteoblast is protective against trabecular bone loss during mechanical unloading, while the effects on cortical bone are more complicated, resulting in preservation of bone formation, while potentially allowing relative structural and material changes that ultimately produce an exaggerated decrease in mechanical properties.

Cx43 cKO mice were generated via an osteocalcin promoter-driven deletion of the gene *Gja1* specifically in osteocytes and osteoblasts (14,28,38). In a previous study, we defined an osteopenic cortical phenotype of these mice characterized by expanded total cross-sectional and marrow area and reduced bone mineral density (14). In the present study, we have confirmed these phenotypic findings and, with a much larger sample size, determined that Cx43 cKO mice also have significantly reduced cortical bone thickness and increased cortical porosity (Figure 2D,F). A comprehensive analysis of baseline trabecular bone parameters revealed no differences, suggesting that a deficiency of Cx43 has a preferential effect on the structural development of cortical bone. This is consistent with other investigations of this model of osteocalcin-driven Cx43 conditional knockout (39), but not those driven by the α_1-collagen promoter, which shows reduced trabecular bone mass (15,40). The differential effect on trabecular structure may be due to the timing of Cx43 deletion in osteoblasts/osteocytes, which occurs later in cell maturation in the osteocalcin-driven model (38). Regardless, the lack of a baseline trabecular phenotype is intriguing, given our findings of selective attenuation of bone loss in this compartment during unloading (Figure 3). It is clear that there are site-specific and loading-specific dependencies of Cx43 on bone structure. The effect of loading environment is highlighted by studies examining the response of Cx43 deficient mice to application of external load: a study examining three point loading of the tibia, to a degree that resulted in woven bone formation, revealed an attenuated anabolic response in Cx43 deficient mice at the endocortical surface (13). However, a more physiological cantilever-loading regimen resulted in increased bone formation and responsiveness in Cx43 deficient mice at the periosteal surface (14). More recently, a study examining the effect of compressive loading confirmed an increased sensitivity to load in Cx43 deficient mice at the periosteal surface (41). These findings highlight the complex nature of Cx43's role in bone homeostasis and the complications inherent in selecting an appropriate animal model.

A recent study by Grimston and colleagues utilized a botulinum toxin (botox) model of muscle immobilization and studied the effects of α_1-collagen-driven Cx43 deficiency on bone loss (15). The investigators demonstrated attenuated cortical bone loss, with no difference in trabecular bone loss. Botox does provide a reasonable model for bone loss associated with immobilization (42), such as that experienced during spinal cord injury or trauma (43). However, unlike the botox model, HLS recapitulates skeletal unloading similar to that experienced during spaceflight, in that it 1) completely eliminates hindlimb ground reaction forces, 2) still allows for passive muscular contractions, and 3) produces a cephalic

fluid shift (25). The latter point is particularly important considering that deleterious changes occur to the vasculature during HLS (44) which result in a reduction in perfusion concomitant to changes in bone mass (45). In addition, differences in the site of attenuated bone loss may be due to differences in the unloading of cortical versus trabecular bone during botox immobilization versus HLS. We observed a much larger ~70% loss of trabecular BV/TV during HLS (Figure 3A), versus ~40% loss during botox immobilization (15); conversely, maximal cortical bone loss (e.g., Ct.Ar) was ~15% for HLS (Figure 5A) versus ~20% botox. From the clinical perspective, reduced physical activity has also been shown to preferentially result in trabecular bone loss, perhaps making the HLS model more applicable to age-related bone loss (17). Regardless, it would be interesting to document the response of animals of the same age and genetic background to both unloading paradigms to determine if these findings represent a model- or genetic-dependent effect, or some combination thereof.

Using an innovative approach, Tatsumi and colleagues were able to demonstrate that diphtheria toxin-induced ablation of osteocytes was able to completely prevent trabecular bone loss in an HLS model of unloading (46). Although the protective effects of Cx43 deficiency presented here were not as complete as the osteocyte ablation model, it is likely that a certain amount of compensatory GJIC from non-Cx43 gap junctions was present. In a previous study, we demonstrated a decrease in gap junction coupling of 80% in primary osteoblasts isolated from cKO mice (14). In addition to GJIC, conditional knockout of Cx43 in this study would have resulted in deletion of Cx43 hemichannels (i.e., “undocked” gap junctions) from osteocytes and osteoblasts (2). Hemichannels have been previously shown to play an important role in mechanotransduction by mediating release of prostaglandins (47) and ATP (48). Cx43 also modulates the MAPK/ERK and PLC pathways (49) and has been shown to interact with structural and signaling molecules such as kinase Src (7,50), protein kinase C-delta (51), and zona occludens-1 (52). Thus, while defective GJIC is certainly an obvious consequence of Cx43 deficiency, and likely to at least partly explain our results, it is possible that alterations in other Cx43 functions contributed to the bone changes that were observed.

There are many parallel pathways mediating skeletal homeostasis during unloading. In addition to completely abolishing osteocyte-osteoblast GJIC, total osteocyte ablation by Tatsumi *et al.* also removed the source of sclerostin (46), an inhibitor of the Wnt/β-catenin pathway (53) that has been implicated as an important mediator of unloading-induced bone loss (54,55). Cx43 is a known target of Wnt/β-catenin signaling (54,56); however, two recent studies have highlighted an additional link between Cx43 and this pathway: a study by Bivi and colleagues found that osteocyte/osteoblast knockout of Cx43 resulted in increased apoptosis of sclerostin-expressing osteocytes (57), while Watkins *et al.* found decreased expression of sclerostin in cortical bone isolated from mice with deletion of Cx43 in the chondro-osteogenic lingeage (58). Thus, the attenuated bone loss seen during unloading in Cx43 deficient mice, whether via botox immobilization or HLS, may be due to decreased expression of sclerostin. Further study of the influence of Cx43 deficiency on the Wnt/β-catenin pathway in the context of unloading will provide additional insight into the mechanisms underlying these findings.

As mentioned, HLS allows for free movement of the hindlimb, similar to the freedom of movement in the “weightless” environment during spaceflight (25,26,59). This movement subjects bony attachments to forces generated during muscle contractions. HLS induces significant muscle atrophy (60), which could contribute to bone loss in this model due to a reduction in muscle contractile forces. Indeed, preservation of muscle mass via exercise (61) or using transgenic animals models (62,63) has been shown to reduce bone loss during unloading. As expected, there was no difference in muscle loss at the gastrocnemius

between genotypes, suggesting that this did not influence the difference in skeletal response between WT and cKO. In addition, we previously quantified ambulation of cKO mice and found no difference in activity level compared to WT (14). Food and water intake and weight loss were also not different between WT and cKO. There were also no baseline differences in body mass or overall body composition between WT and cKO mice, which is consistent with previous studies using the osteocalcin-driven Cx43 cKO model (38).

Despite their cortical osteopenic phenotype, femurs from cKO mice were found to exhibit greater structural strength and ultimate bending energy than those from WT at baseline (Figure 6C, E). Analysis of microCT data revealed a greater cortical bone area and calculated pMOI for cKO versus WT (Figure 6A). Although tissue stiffness was not directly measured, it is likely that this was decreased in the cKO animals consistent with the lower cortical BMD. Whereas the increased cortical area and pMOI appear dominant in increasing ultimate moment and energy withstood by the cKO bones, bending rigidity was similar to WT, consistent with the decreased tissue stiffness combined with the aforementioned increased pMOI. These findings stand in contrast to those we documented in this same strain of mice at eight weeks of age, where cKO were significantly weaker than WT (14). It appears that cortical expansion, a natural consequence of aging (64,65), occurs more rapidly in cKO mice, ultimately resulting in greater equalization of bone strength. Study of older cKO mice is necessary to document changes in the cortical and trabecular phenotype with more advanced aging and to determine concomitant changes in strength, structural, and material properties.

Compared to trabecular bone loss, cortical bone loss as assessed by microCT was modest and similar between genotypes (Figure 5). Despite these similar structural changes, there was a greater relative difference between normally loaded and unloaded femurs with regards to strength, bending rigidity, and ultimate energy (Figure 6C-E). These findings suggest that the relationship between structural change and strength outcomes are non-linear, resulting in a greater decrease in strength in cKO mice. It is important to note that the structure of cKO femurs starts out in a much different state from that of WT (Figure 2). With expanded cortices, cortical thinning, and increased porosity, it is clear that losing a similar amount of bone resulted in a relatively greater effect on cKO mechanical properties in this test paradigm. In addition, it may be that there was a differential effect of unloading on the material properties of cKO mice. Although not measured, greater changes in the collagen content or the ratio of lamellar to woven bone could have all contributed to the effects that were observed (65,66). For example, although it was not significant, it does appear that cortical BMD decreased to a greater degree during unloading of cKO mice versus WT (Figure 5E). Bivi and colleagues have shown increased baseline osteocyte apoptosis in cKO deficient bones (57), while HLS itself has been shown to reduce osteocyte number (67). Reduced osteocyte viability has been correlated to impaired bone repair (68), the accumulation of microcracks (69,70), and the increased fracture risk (71). It may be that in this age and strain of mice the effect of osteocyte deficiency was not enough to result in lower baseline strength, but did contribute to greater deleterious changes in bone quality and material properties, and thus mechanical properties, during unloading. Finally, we cannot discount that the aforementioned convoluted endocortical surface of cortical bone in cKO mice (Figure 2G) created stress concentrations that contributed more negatively to bone integrity following unloading.

In the present study, we observed profound suppression of bone formation, particularly at the endocortical surface, in mice subjected to unloading (Figure 7). Deficiency of Cx43 was able to completely ameliorate this effect and preserve bone formation. The total perimeter undergoing active mineralization as well as the mineral apposition rate was also preserved in cKO mice subjected to unloading. There findings are consistent with similar studies of HLS

unloading in mice with osteocyte ablation (46) or sclerostin knockout (54), as well as Cx43 deficiency during botox immobilization (41). Despite the dramatic preservation of bone formation, we did not observe preservation of cortical bone structure during unloading of cKO mice. It is important to note, however, that the labeling technique utilized only allows for quantification of new bone formed between administration of the Calcein and alizarin red labels (i.e., 2 weeks). In the case of skeletally mature mice, such as those with a C57BL/6 background used presently, baseline bone formation is substantially lower than that found in younger animals (54). As a result, even though bone formation was preserved in cKO mice, the resultant difference in cortical bone structure was apparently not enough to meet the detection threshold of the imaging techniques utilized. This is evident by the finding of little to no changes in cortical bone parameters due to natural growth of WT or cKO normally loaded control mice over the experimental period (Figure 5). Indeed, the fact that bone loss still occurs despite the maintenance of bone formation in cKO mice indicates that bone loss was predominantly the result of increased bone resorption. Such a conclusion is not unexpected, and was indeed one of the primary reasons for selecting skeletally mature animals. Ultimately, we sought to simulate spaceflight or bed rest disuse occurring in a skeletally mature astronaut or clinical population, rather than focusing on inhibition of bone formation and growth as would be expected with use of younger animals (e.g., 8-12 weeks) (72). Quantification of eroded surface in these mice could have provided insight in to the bone resorption dynamics, however, the presence of the highly convoluted endocortical border of cKO mice prevented accurate assessment of this parameter. This scalloped surface is similar to that observed in a previous study of Dermo1 promoter-driven Cx43 knockout (58), and is likely due to increased endosteal osteoclast-mediated bone resorption. In addition, it is worth noting that there were no differences between WT and cKO control mice in regards to endocortical bone formation parameters, while at the periosteal surface we observed lower MAR and BFR/BS in cKO mice versus WT (Figure 7E,F). These findings are opposite of those found in the ulna of Cx43 cKO mice from a previous study we conducted (14). Aside from the different bone investigated, our previous study also utilized a shorter labeling period (6 vs. 14 days). In addition, mice in the present study were housed in wire-bottom cages that may have induced changes in animal activity, behavior, and loading versus standard vivarium cages, such as that observed in ground-based use of spaceflight animal enclosures (73,74). Regardless, these contrasting findings highlight the potential for bone-specific and site-specific effects of Cx43 in bone homeostasis.

The results of the present study demonstrate, for the first time, the response of Cx43 deficient mice to the HLS unloading paradigm. We have demonstrated that a lack of Cx43 in bone cells protects against trabecular bone loss and suppression of cortical bone formation during unloading. Cortical bone structure, however, was not protected during unloading and there was observed a relatively greater decrease in the mechanical properties of femurs from cKO mice. This observation may be the result of a differential effect of unloading on the material properties of bone from cKO mice. Combined with previous studies demonstrating increased responsiveness of Cx43 deficient bone to mechanical loading (14,41), a model of Cx43 deficiency is emerging whereby it reduces sensitivity to unloading (15) and increases sensitivity to loading (14,41). This may have important implications in the development of Cx43 as a therapeutic target for the prevention of bone loss associated with unloading, disuse, or aging.

Acknowledgments

This work was supported by grant R01 AG013087 from the National Institute on Aging, and R03 AR057546 from the National Institute of Arthritis and Musculoskeletal and Skin Diseases, National Institutes of Health. Thanks to Dr. Arthur Berg, PhD, Assistant Professor of Biostatistics and Bioinformatics at the Penn State College of Medicine for providing assistance with the statistical analysis. Thanks to Dr. Charles Lang for providing assistance with

muscle and ^{1}H-NMR body composition analyses. This manuscript is dedicated to the memory of Catherine Donahue.

REFERENCES

1. Jiang JX, Siller-Jackson AJ, Burra S. Roles of gap junctions and hemichannels in bone cell functions and in signal transmission of mechanical stress. Frontiers in bioscience: a journal and virtual library. 2007; 12:1450–1462. [PubMed: 17127393]
2. Goodenough DA, Paul DL. Beyond the gap: functions of unpaired connexon channels. Nature reviews Molecular cell biology. 2003; 4(4):285–294.
3. Civitelli R, Beyer EC, Warlow PM, Robertson AJ, Geist ST, Steinberg TH. Connexin43 mediates direct intercellular communication in human osteoblastic cell networks. Journal of Clinical Investigation. 1993; 91(5):1888–1896. [PubMed: 8387535]
4. Donahue HJ. Gap junctions and biophysical regulation of bone cell differentiation. Bone. 2000; 26(5):417–422. [PubMed: 10773579]
5. Schilling AF, Filke S, Lange T, Gebauer M, Brink S, Baranowsky A, Zustin J, Amling M. Gap Junctional Communication in Human Osteoclasts in vitro and in vivo. J Cell Mol Med. 2008
6. Alford AI, Jacobs CR, Donahue HJ. Oscillating fluid flow regulates gap junction communication in osteocytic MLO-Y4 cells by an ERK1/2 MAP kinase-dependent mechanism. Bone. 2003; 33(1):64–70. [PubMed: 12919700]
7. Plotkin LI, Weinstein RS, Parfitt AM, Roberson PK, Manolagas SC, Bellido T. Prevention of osteocyte and osteoblast apoptosis by bisphosphonates and calcitonin. The Journal of clinical investigation. 1999; 104(10):1363–1374. [PubMed: 10562298]
8. Bivi N, Lezcano V, Romanello M, Bellido T, Plotkin LI. Connexin43 interacts with betaarrestin: a pre-requisite for osteoblast survival induced by parathyroid hormone. Journal of cellular biochemistry. 2011; 112(10):2920–2930. [PubMed: 21630325]
9. Stains JP, Lecanda F, Screen J, Towler DA, Civitelli R. Gap junctional communication modulates gene transcription by altering the recruitment of Sp1 and Sp3 to connexin-response elements in osteoblast promoters. The Journal of biological chemistry. 2003; 278(27):24377–24387. [PubMed: 12700237]
10. Paznekas WA, Karczeski B, Vermeer S, Lowry RB, Delatycki M, Laurence F, Koivisto PA, Van Maldergem L, Boyadjiev SA, Bodurtha JN, Jabs EW. GJA1 mutations, variants, and connexin 43 dysfunction as it relates to the oculodentodigital dysplasia phenotype. Hum Mutat. 2009; 30(5): 724–733. [PubMed: 19338053]
11. Taylor AF, Saunders MM, Shingle DL, Cimbala JM, Zhou Z, Donahue HJ. Mechanically stimulated osteocytes regulate osteoblastic activity via gap junctions. Am J Physiol Cell Physiol. 2007; 292(1):C545–552. [PubMed: 16885390]
12. Grimston SK, Screen J, Haskell JH, Chung DJ, Brodt MD, Silva MJ, Civitelli R. Role of connexin43 in osteoblast response to physical load. Ann N Y Acad Sci. 2006; 1068:214–224. [PubMed: 16831921]
13. Grimston SK, Brodt MD, Silva MJ, Civitelli R. Attenuated response to in vivo mechanical loading in mice with conditional osteoblast ablation of the connexin43 gene (Gja1). Journal of bone and mineral research: the official journal of the American Society for Bone and Mineral Research. 2008; 23(6):879–886. [PubMed: 18282131]
14. Zhang Y, Paul EM, Sathyendra V, Davison A, Sharkey N, Bronson S, Srinivasan S, Gross TS, Donahue HJ. Enhanced osteoclastic resorption and responsiveness to mechanical load in gap junction deficient bone. PloS one. 2011; 6(8):e23516. [PubMed: 21897843]
15. Grimston SK, Goldberg DB, Watkins M, Brodt MD, Silva MJ, Civitelli R. Connexin43 deficiency reduces the sensitivity of cortical bone to the effects of muscle paralysis. Journal of bone and mineral research: the official journal of the American Society for Bone and Mineral Research. 2011; 26(9):2151–2160. [PubMed: 21590735]
16. Maimoun L, Fattal C, Micallef JP, Peruchon E, Rabischong P. Bone loss in spinal cord-injured patients: from physiopathology to therapy. Spinal cord. 2006; 44(4):203–210. [PubMed: 16158075]

17. Tervo T, Nordstrom P, Neovius M, Nordstrom A. Reduced physical activity corresponds with greater bone loss at the trabecular than the cortical bone sites in men. Bone. 2009; 45(6):1073–1078. [PubMed: 19631302]

18. Bloomfield SA. Disuse osteopenia. Current osteoporosis reports. 2010; 8(2):91–97. [PubMed: 20425616]

19. Beller G, Belavy DL, Sun L, Armbrecht G, Alexandre C, Felsenberg D. WISE-2005: bed-rest induced changes in bone mineral density in women during 60 days simulated microgravity. Bone. 2011; 49(4):858–866. [PubMed: 21723970]

20. Rittweger J, Simunic B, Bilancio G, De Santo NG, Cirillo M, Biolo G, Pisot R, Eiken O, Mekjavic IB, Narici M. Bone loss in the lower leg during 35 days of bed rest is predominantly from the cortical compartment. Bone. 2009; 44(4):612–618. [PubMed: 19168165]

21. Lang T, LeBlanc A, Evans H, Lu Y, Genant H, Yu A. Cortical and trabecular bone mineral loss from the spine and hip in long-duration spaceflight. Journal of bone and mineral research: the official journal of the American Society for Bone and Mineral Research. 2004; 19(6):1006–1012. [PubMed: 15125798]

22. Lang TF, Leblanc AD, Evans HJ, Lu Y. Adaptation of the proximal femur to skeletal reloading after long-duration spaceflight. Journal of bone and mineral research: the official journal of the American Society for Bone and Mineral Research. 2006; 21(8):1224–1230. [PubMed: 16869720]

23. Lang TF. What do we know about fracture risk in long-duration spaceflight? Journal of musculoskeletal & neuronal interactions. 2006; 6(4):319–321. [PubMed: 17185806]

24. Kanis J, Oden A, Johnell O. Acute and long-term increase in fracture risk after hospitalization for stroke. Stroke; a journal of cerebral circulation. 2001; 32(3):702–706.

25. Morey-Holton ER. Hindlimb unloading rodent model: technical aspects. Journal of applied physiology. 2002; 92(4):1367–1377. [PubMed: 11895999]

26. Bikle DD, Halloran BP. The response of bone to unloading. Journal of bone and mineral metabolism. 1999; 17(4):233–244. [PubMed: 10575587]

27. Zhang M, Xuan S, Bouxsein ML, von Stechow D, Akeno N, Faugere MC, Malluche H, Zhao G, Rosen CJ, Efstratiadis A, Clemens TL. Osteoblast-specific knockout of the insulin-like growth factor (IGF) receptor gene reveals an essential role of IGF signaling in bone matrix mineralization. J Biol Chem. 2002; 277(46):44005–44012. [PubMed: 12215457]

28. Castro CH, Stains JP, Sheikh S, Szejnfeld VL, Willecke K, Theis M, Civitelli R. Development of mice with osteoblast-specific connexin43 gene deletion. Cell communication & adhesion. 2003; 10(4-6):445–450. [PubMed: 14681055]

29. Hargens AR, Steskal J, Johansson C, Tipton CM. Tissue fluid shift, forelimb loading, and tail tension in tail suspended rats. Physiologist. 1984; 27:S37–S38.

30. Klinck RJ, Campbell GM, Boyd SK. Radiation effects on bone architecture in mice and rats resulting from in vivo micro-computed tomography scanning. Medical engineering & physics. 2008; 30(7):888–895. [PubMed: 18249025]

31. Bouxsein ML, Boyd SK, Christiansen BA, Guldberg RE, Jepsen KJ, Muller R. Guidelines for assessment of bone microstructure in rodents using micro-computed tomography. Journal of bone and mineral research: the official journal of the American Society for Bone and Mineral Research. 2010; 25(7):1468–1486. [PubMed: 20533309]

32. Lang DH, Sharkey NA, Lionikas A, Mack HA, Larsson L, Vogler GP, Vandenbergh DJ, Blizard DA, Stout JT, Stitt JP, McClearn GE. Adjusting data to body size: a comparison of methods as applied to quantitative trait loci analysis of musculoskeletal phenotypes. J Bone Miner Res. 2005; 20(5):748–757. [PubMed: 15824847]

33. Brodt MD, Ellis CB, Silva MJ. Growing C57Bl/6 mice increase whole bone mechanical properties by increasing geometric and material properties. Journal of bone and mineral research: the official journal of the American Society for Bone and Mineral Research. 1999; 14(12):2159–2166. [PubMed: 10620076]

34. Silva MJ, Brodt MD, Lynch MA, McKenzie JA, Tanouye KM, Nyman JS, Wang X. Type 1 diabetes in young rats leads to progressive trabecular bone loss, cessation of cortical bone growth, and diminished whole bone strength and fatigue life. Journal of bone and mineral research: the

official journal of the American Society for Bone and Mineral Research. 2009; 24(9):1618–1627. [PubMed: 19338453]

35. Li J, Liu D, Ke HZ, Duncan RL, Turner CH. The P2X7 nucleotide receptor mediates skeletal mechanotransduction. J Biol Chem. 2005; 280(52):42952–42959. [PubMed: 16269410]
36. Parfitt AM, Drezner MK, Glorieux FH, Kanis JA, Malluche H, Meunier PJ, Ott SM, Recker RR. Bone histomorphometry: standardization of nomenclature, symbols, and units. Report of the ASBMR Histomorphometry Nomenclature Committee. Journal of bone and mineral research: the official journal of the American Society for Bone and Mineral Research. 1987; 2(6):595–610.
37. Lang CH, Frost RA, Bronson SK, Lynch CJ, Vary TC. Skeletal muscle protein balance in mTOR heterozygous mice in response to inflammation and leucine. American journal of physiology Endocrinology and metabolism. 2010; 298(6):E1283–1294. [PubMed: 20388826]
38. Plotkin LI, Lezcano V, Thostenson J, Weinstein RS, Manolagas SC, Bellido T. Connexin 43 is required for the anti-apoptotic effect of bisphosphonates on osteocytes and osteoblasts in vivo. Journal of bone and mineral research: the official journal of the American Society for Bone and Mineral Research. 2008; 23(11):1712–1721. [PubMed: 18597631]
39. Bivi N, Aguirre JI, Vyas K, Allen M, Bellido T, Plotkin L. Increased osteocyte apoptosis and bone resorption, and decreased strength of cortical but not trabecular bone in mice lacking connexin43 in osteoblasts and osteocytes. J Bone Miner Res. 2009; 24(Suppl 1) Avaialble at http://onlinelibrary.wiley.com/doi/10.1002/jbmr.5650241301/full.
40. Chung DJ, Castro CH, Watkins M, Stains JP, Chung MY, Szejnfeld VL, Willecke K, Theis M, Civitelli R. Low peak bone mass and attenuated anabolic response to parathyroid hormone in mice with an osteoblast-specific deletion of connexin43. Journal of cell science. 2006; 119(Pt 20):4187–4198. [PubMed: 16984976]
41. Grimston, SK.; Watkins, M.; Brodt, M.; Silva, M.; Civitelli, R. Variable Bone Formation Response to Skeletal Axial Load in Mice With a Conditional Deletion of the Connexin43 (Cx43) Gene (Gja1) 2011 Annual Meeting of the American Society of Bone and Mineral Research; San Diego, CA. 2011; p. S75
42. Grimston SK, Silva MJ, Civitelli R. Bone loss after temporarily induced muscle paralysis by Botox is not fully recovered after 12 weeks. Annals of the New York Academy of Sciences. 2007; 1116:444–460. [PubMed: 17584988]
43. Qin W, Bauman WA, Cardozo C. Bone and muscle loss after spinal cord injury: organ interactions. Annals of the New York Academy of Sciences. 2010; 1211:66–84. [PubMed: 21062296]
44. Delp MD, Colleran PN, Wilkerson MK, McCurdy MR, Muller-Delp J. Structural and functional remodeling of skeletal muscle microvasculature is induced by simulated microgravity. American journal of physiology Heart and circulatory physiology. 2000; 278(6):H1866–1873. [PubMed: 10843883]
45. Colleran PN, Wilkerson MK, Bloomfield SA, Suva LJ, Turner RT, Delp MD. Alterations in skeletal perfusion with simulated microgravity: a possible mechanism for bone remodeling. Journal of applied physiology. 2000; 89(3):1046–1054. [PubMed: 10956349]
46. Tatsumi S, Ishii K, Amizuka N, Li M, Kobayashi T, Kohno K, Ito M, Takeshita S, Ikeda K. Targeted ablation of osteocytes induces osteoporosis with defective mechanotransduction. Cell metabolism. 2007; 5(6):464–475. [PubMed: 17550781]
47. Siller-Jackson AJ, Burra S, Gu S, Xia X, Bonewald LF, Sprague E, Jiang JX. Adaptation of connexin 43-hemichannel prostaglandin release to mechanical loading. The Journal of biological chemistry. 2008; 283(39):26374–26382. [PubMed: 18676366]
48. Genetos DC, Kephart CJ, Zhang Y, Yellowley CE, Donahue HJ. Oscillating fluid flow activation of gap junction hemichannels induces ATP release from MLO-Y4 osteocytes. Journal of cellular physiology. 2007; 212(1):207–214. [PubMed: 17301958]
49. Civitelli R. Cell-cell communication in the osteoblast/osteocyte lineage. Archives of biochemistry and biophysics. 2008; 473(2):188–192. [PubMed: 18424255]
50. Giepmans BN, Hengeveld T, Postma FR, Moolenaar WH. Interaction of c-Src with gap junction protein connexin-43. Role in the regulation of cell-cell communication. The Journal of biological chemistry. 2001; 276(11):8544–8549.

51. Niger C, Hebert C, Stains JP. Interaction of connexin43 and protein kinase C-delta during FGF2 signaling. BMC biochemistry. 2010; 11:14. [PubMed: 20338032]
52. Laing JG, Chou BC, Steinberg TH. ZO-1 alters the plasma membrane localization and function of Cx43 in osteoblastic cells. Journal of cell science. 2005; 118(Pt 10):2167–2176. [PubMed: 15855237]
53. Poole KE, van Bezooijen RL, Loveridge N, Hamersma H, Papapoulos SE, Lowik CW, Reeve J. Sclerostin is a delayed secreted product of osteocytes that inhibits bone formation. FASEB journal: official publication of the Federation of American Societies for Experimental Biology. 2005; 19(13):1842–1844. [PubMed: 16123173]
54. Lin C, Jiang X, Dai Z, Guo X, Weng T, Wang J, Li Y, Feng G, Gao X, He L. Sclerostin mediates bone response to mechanical unloading through antagonizing Wnt/beta-catenin signaling. Journal of bone and mineral research: the official journal of the American Society for Bone and Mineral Research. 2009; 24(10):1651–1661. [PubMed: 19419300]
55. Tian X, Jee WS, Li X, Paszty C, Ke HZ. Sclerostin antibody increases bone mass by stimulating bone formation and inhibiting bone resorption in a hindlimb-immobilization rat model. Bone. 2011; 48(2):197–201. [PubMed: 20850580]
56. Rucci N, Rufo A, Alamanou M, Teti A. Modeled microgravity stimulates osteoclastogenesis and bone resorption by increasing osteoblast RANKL/OPG ratio. Journal of cellular biochemistry. 2007; 100(2):464–473. [PubMed: 16927271]
57. Bivi N, Condon KW, Allen MR, Farlow N, Passeri G, Brun LR, Rhee Y, Bellido T, Plotkin LI. Cell autonomous requirement of connexin 43 for osteocyte survival: consequences for endocortical resorption and periosteal bone formation. Journal of bone and mineral research: the official journal of the American Society for Bone and Mineral Research. 2012; 27(2):374–389. [PubMed: 22028311]
58. Watkins M, Grimston SK, Norris JY, Guillotin B, Shaw A, Beniash E, Civitelli R. Osteoblast connexin43 modulates skeletal architecture by regulating both arms of bone remodeling. Molecular biology of the cell. 2011; 22(8):1240–1251. [PubMed: 21346198]
59. Morey-Holton E, Globus RK, Kaplansky A, Durnova G. The hindlimb unloading rat model: literature overview, technique update and comparison with space flight data. Advances in space biology and medicine. 2005; 10:7–40. [PubMed: 16101103]
60. Hurst JE, Fitts RH. Hindlimb unloading-induced muscle atrophy and loss of function: protective effect of isometric exercise. Journal of applied physiology. 2003; 95(4):1405–1417. [PubMed: 12819219]
61. Cavanagh PR, Licata AA, Rice AJ. Exercise and pharmacological countermeasures for bone loss during long-duration space flight. Gravitational and space biology bulletin: publication of the American Society for Gravitational and Space Biology. 2005; 18(2):39–58. [PubMed: 16038092]
62. Kondo H, Ezura Y, Nakamoto T, Hayata T, Notomi T, Sorimachi H, Takeda S, Noda M. MURF1 deficiency suppresses unloading-induced effects on osteoblasts and osteoclasts to lead to bone loss. Journal of cellular biochemistry. 2011; 112(12):3525–3530. [PubMed: 21866567]
63. Elkasrawy MN, Hamrick MW. Myostatin (GDF-8) as a key factor linking muscle mass and bone structure. Journal of musculoskeletal & neuronal interactions. 2010; 10(1):56–63. [PubMed: 20190380]
64. Iwamoto J, Takeda T, Otani T, Yabe Y. Age-related changes in cortical bone in women: metacarpal bone mass measurement study. Journal of orthopaedic science: official journal of the Japanese Orthopaedic Association. 1998; 3(2):90–94. [PubMed: 9654561]
65. Augat P, Schorlemmer S. The role of cortical bone and its microstructure in bone strength. Age and ageing. 2006; 35(Suppl 2):ii27–ii31. [PubMed: 16926200]
66. Davison KS, Siminoski K, Adachi JD, Hanley DA, Goltzman D, Hodsman AB, Josse R, Kaiser S, Olszynski WP, Papaioannou A, Ste-Marie LG, Kendler DL, Tenenhouse A, Brown JP. Bone strength: the whole is greater than the sum of its parts. Seminars in arthritis and rheumatism. 2006; 36(1):22–31. [PubMed: 16887465]
67. Aguirre JI, Plotkin LI, Stewart SA, Weinstein RS, Parfitt AM, Manolagas SC, Bellido T. Osteocyte apoptosis is induced by weightlessness in mice and precedes osteoclast recruitment and bone loss.

Journal of bone and mineral research: the official journal of the American Society for Bone and Mineral Research. 2006; 21(4):605–615. [PubMed: 16598381]

68. Dunstan CR, Somers NM, Evans RA. Osteocyte death and hip fracture. Calcified tissue international. 1993; 53(Suppl 1):S113–116. discussion S116-117. [PubMed: 8275364]
69. Mori S, Harruff R, Ambrosius W, Burr DB. Trabecular bone volume and microdamage accumulation in the femoral heads of women with and without femoral neck fractures. Bone. 1997; 21(6):521–526. [PubMed: 9430242]
70. Vashishth D, Verborgt O, Divine G, Schaffler MB, Fyhrie DP. Decline in osteocyte lacunar density in human cortical bone is associated with accumulation of microcracks with age. Bone. 2000; 26(4):375–380. [PubMed: 10719281]
71. Qiu S, Rao DS, Palnitkar S, Parfitt AM. Reduced iliac cancellous osteocyte density in patients with osteoporotic vertebral fracture. Journal of bone and mineral research: the official journal of the American Society for Bone and Mineral Research. 2003; 18(9):1657–1663. [PubMed: 12968675]
72. Lloyd SA, Travis ND, Lu T, Bateman TA. Development of a low-dose anti-resorptive drug regimen reveals synergistic suppression of bone formation when coupled with disuse. Journal of applied physiology. 2008; 104(3):729–738. [PubMed: 18174391]
73. Lloyd, SA.; Ferguson, VL.; Simske, SJ.; Dunlap, A.; Livingston, E.; Bateman, TA. Effects of Animal Enclosure Module Spaceflight Hardware on the Skeletal Properties of Ground Control Mice 2011 Annual Meeting of the American Society of Bone and Mineral Research; Toronto, Canada. 2010.
74. Morey-Holton ER, Halloran BP, Garetto LP, Doty SB. Animal housing influences the response of bone to spaceflight in juvenile rats. Journal of applied physiology. 2000; 88(4):1303–1309. [PubMed: 10749823]

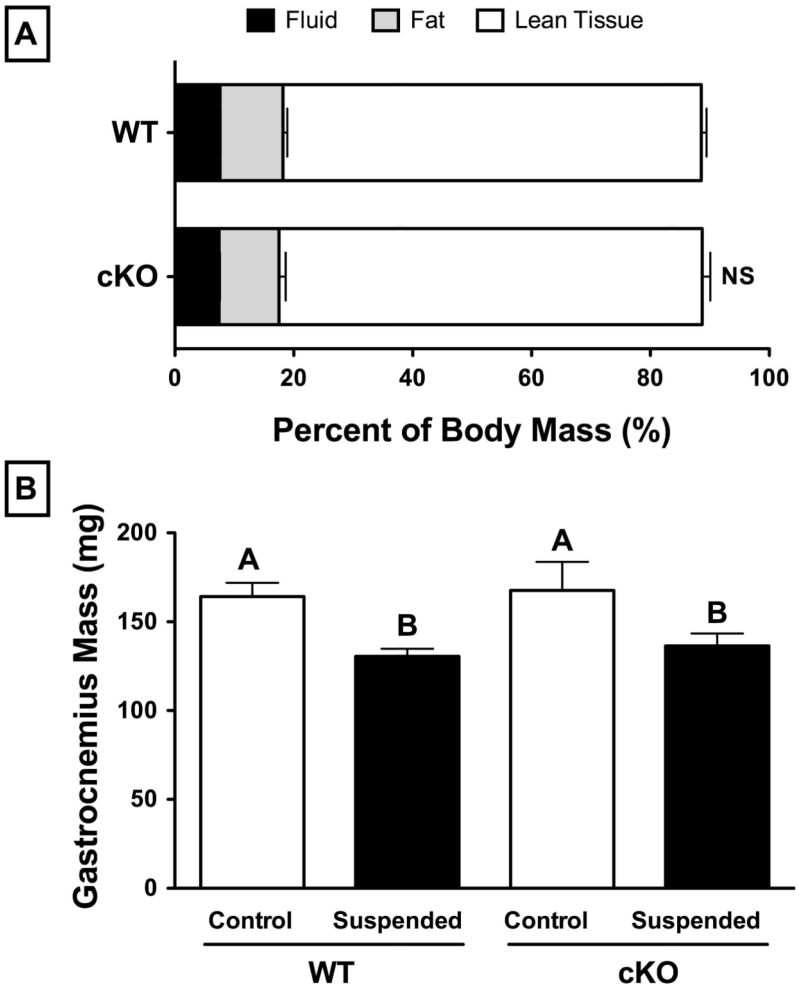

Figure 1.

(A) Comparison of baseline body composition between 6-month old, male wild-type (WT) and Cx43 conditional knockout (cKO) mice as assessed by H^1-NMR. There were no significant differences with respect to fluid mass (7-8%), fat mass (10-11%), or lean mass (70-71%) ($p>0.05$ of WT versus cKO via t-test). (B) Gastrocnemius muscle wet mass of WT and cKO mice under control and suspended conditions. There was no difference between genotypes within the control group, while muscle mass in mice following suspension was ~20% less than their respective normally loaded control ($p<0.05$ via two-way ANOVA). Mean±SE. Different letters indicate significant difference, while similar letters indicate no difference.

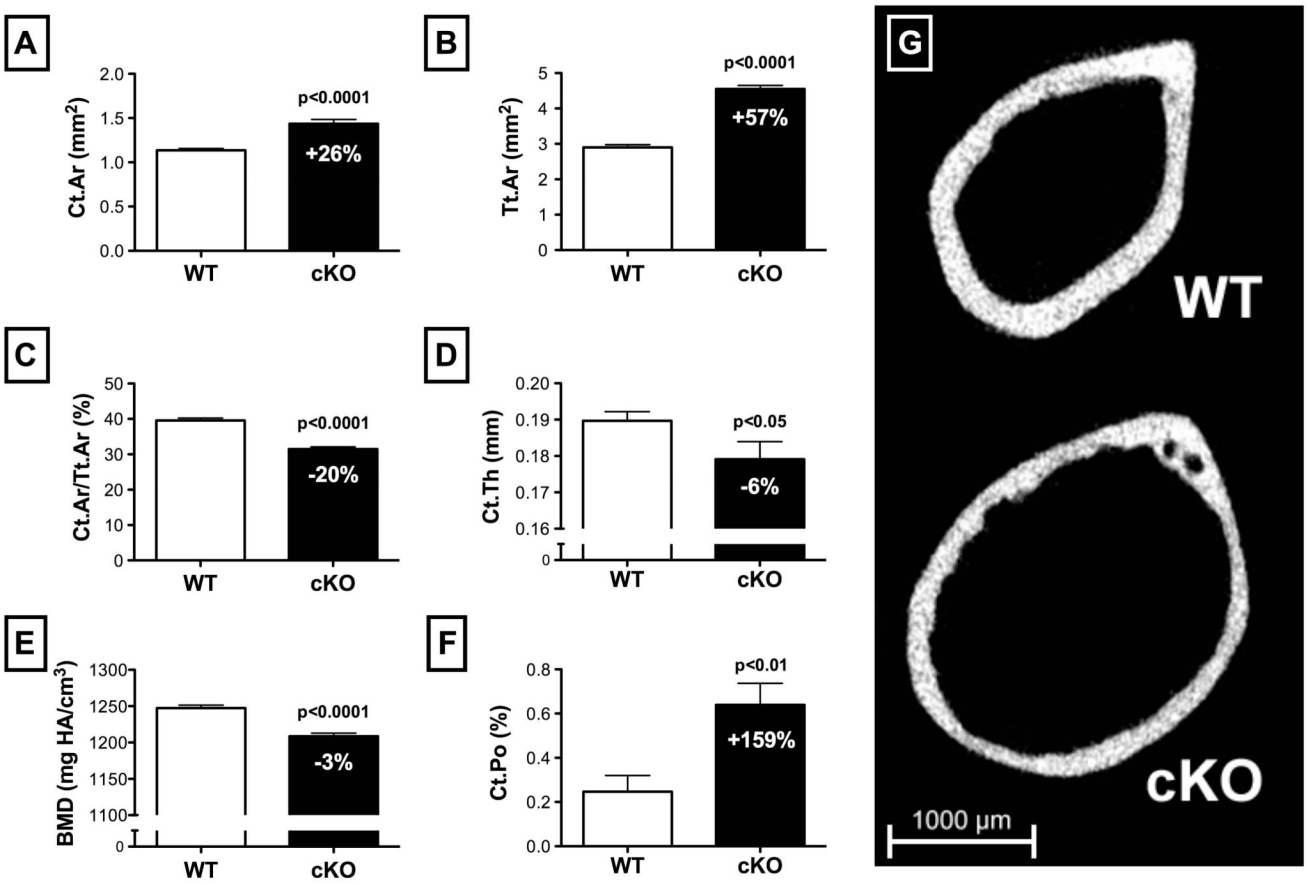

Figure 2.

Comparison of baseline cortical bone structure between 6-month-old, male wild-type (WT) and Cx43 conditional knockout (cKO) mice assessed by a microCT scan of the mid-shaft of the femur (n=25-30 per genotype). (A) Cortical bone area (Ct.Ar) and (B) total cross-sectional area (Tt.Ar) were both increased in cKO versus WT, although the latter to a greater extent, resulting in relatively lower (C) cortical area fraction (Ct.Ar/Tt.Ar) ($p<0.0001$ for all). (D) Cortical thickness (Ct.Th) was lower in cKO versus WT ($p<0.05$), as was (E) cortical bone mineral density (BMD) ($p<0.0001$), and (F) cortical porosity (Ct.Po) ($p<0.01$). (G) A representative 2D microCT image highlights the aforementioned osteopenic phenotype. Comparisons via t-test. Mean±SE.

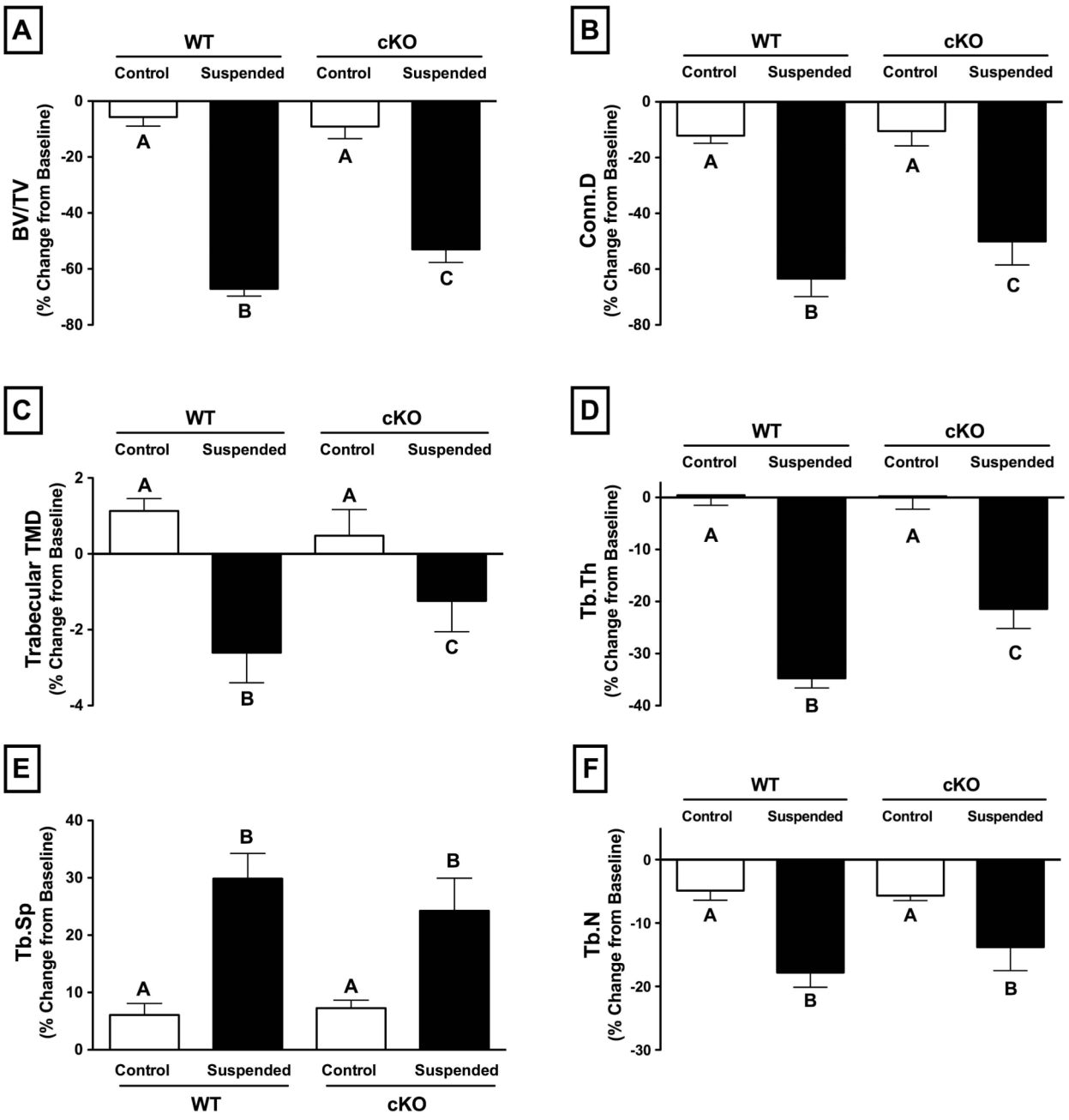

Figure 3.

Change in trabecular bone parameters in wild-type (WT) and Cx43 conditional knockout (cKO) mice following three weeks of normal loading conditions (Control) or mechanical unloading via hindlimb suspension (Suspended). Significant decreases were seen in all measured parameters in WT Suspended animals, with the effect significantly attenuated in cKO for (A) trabecular bone volume fraction (BV/TV; $p<0.01$), (B) connectivity density (Conn.D; $p<0.05$), (C) trabecular bone mineral density (BMD; $p<0.05$), (D) trabecular thickness (Tb.Th; $p<0.001$). The difference between Suspended WT and cKO for (E) trabecular separation (Tb.Sp) and (F) trabecular number (Tb.N) was not significant, although there were statistical trends ($p=0.1$ and $p=0.15$, respectively) suggesting a similar

attenuated loss of trabecular microstructure in cKO mice subjected to unloading. Comparisons via two-way ANOVA. Mean±SE. Different letters indicate significant difference, while similar letters indicate no difference.

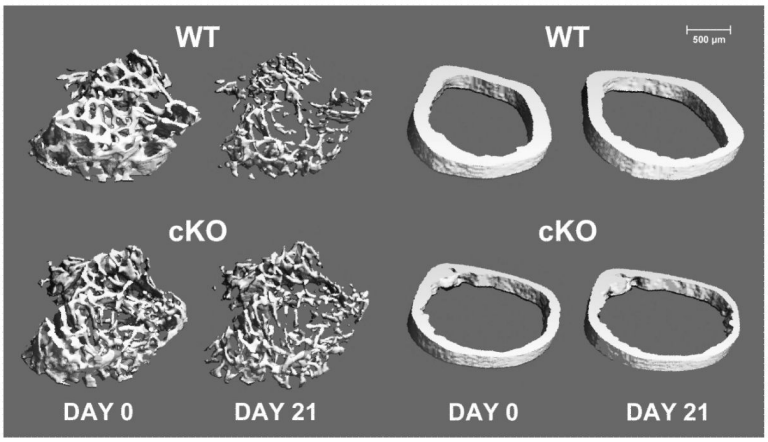

Figure 4.

Trabecular (left) and cortical (right) microstructure in wild-type (WT) and Cx43 conditional knockout (cKO) mice at baseline (Day 0) and following three weeks of mechanical unloading via hindlimb suspension (Day 21). Representative 3D microCT reconstructions were selected based on mean loss of trabecular BV/TV and cortical thickness for each genotype. Trabecular images represent 72 slices (756 μm) of the proximal tibia, immediately distal to the epiphyseal plate. Cortical images represent 22 slices (231 μm) of the femur midshaft. Significant degradation of trabecular microstructure can be observed in WT following unloading, with an attenuated response in cKO. The effect of unloading on cortical microstructure is subtler, with similar effects on both WT and cKO.

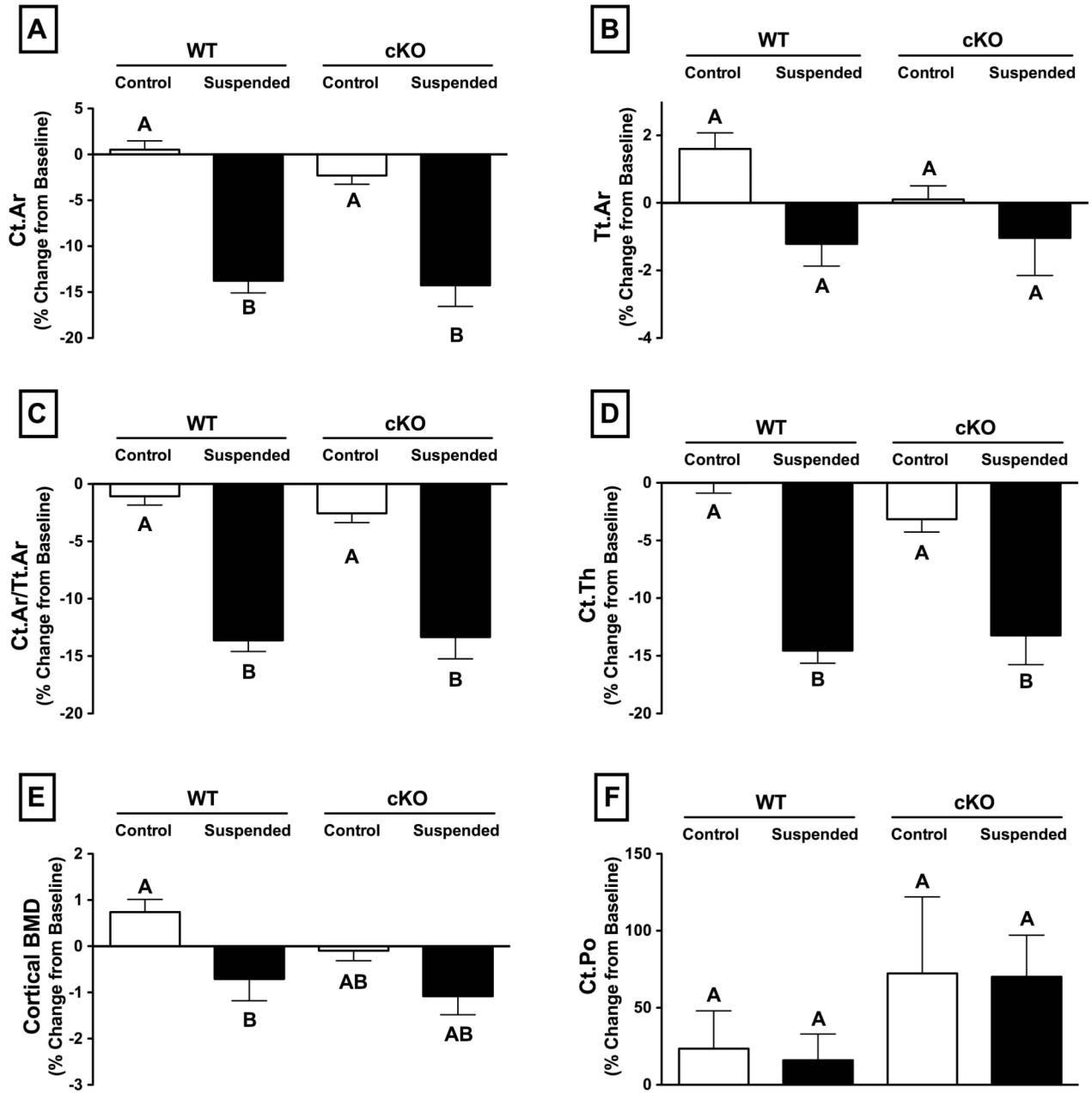

Figure 5.

Change in cortical bone parameters in wild-type (WT) and Cx43 conditional knockout (cKO) mice following three weeks of normal loading conditions (Control) or mechanical unloading via hindlimb suspension (Suspended). There was degradation of cortical microstructure with unloading, as indicated by significant decreases in several measured parameters, although there was no difference between WT and cKO for any measured parameters. (A) cortical area (Ct.Ar), (B) total cross-sectional area (Tt.Ar), (C) cortical area fraction (Ct.Ar/Tt.Ar), (D) cortical thickness (Ct.Th), (E) cortical bone mineral density (BMD), (F) cortical porosity (Ct.Po). Comparisons via two-way ANOVA. Mean±SE. Different letters indicate significant difference, while similar letters indicate no difference.

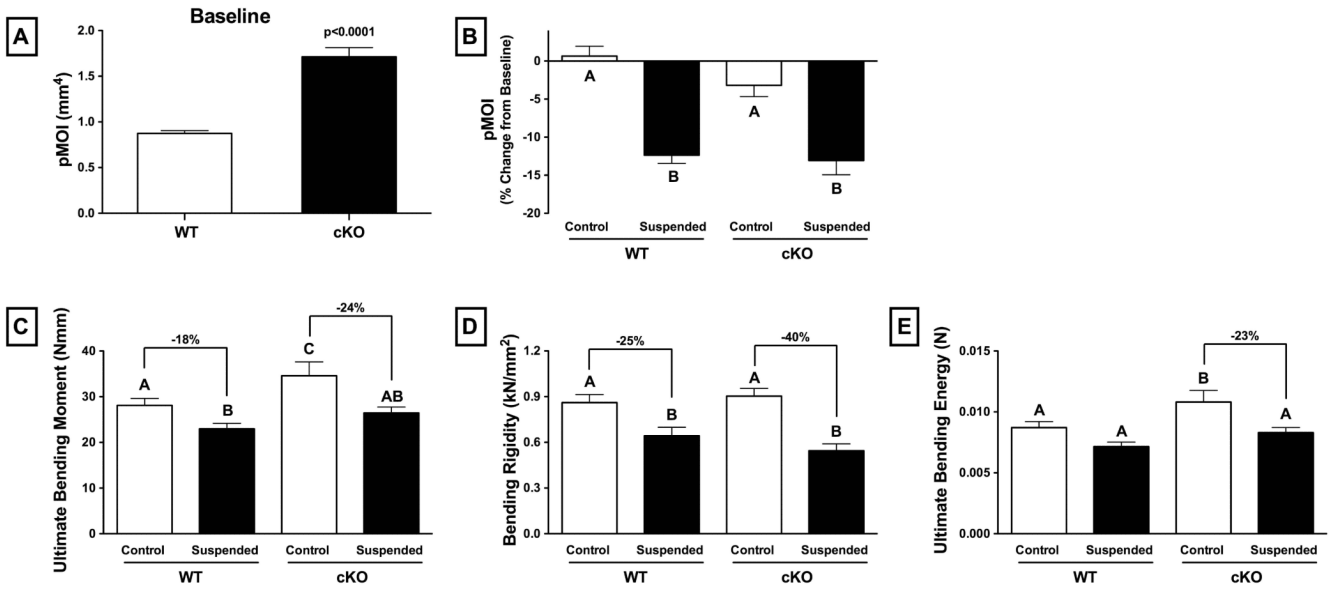

Figure 6.

Geometric and mechanical properties of wild-type (WT) and Cx43 conditional knockout (cKO) mice as assessed by MicroCT and mechanical testing. At baseline, femurs from cKO mice have significantly greater (A) polar moment of inertia (pMOI) ($p<0.0001$). Femurs were collected from mice following three weeks of normal loading (Control) or mechanical unloading via hindlimb suspension (Suspended) and tested to failure in a three-point bending paradigm. As a result of unloading, WT and cKO experienced a similar decrease in (B) pMOI ($p>0.05$ via two-way ANOVA). (C) Ultimate bending moment (i.e., strength) was significantly lower in Suspended versus Control, although the difference was greater for cKO mice. There were similar findings for (D) bending rigidity and (E) ultimate bending energy ($p<0.05$ via two-way ANOVA). Mean±SE. Different letters indicate significant difference, while similar letters indicate no difference.

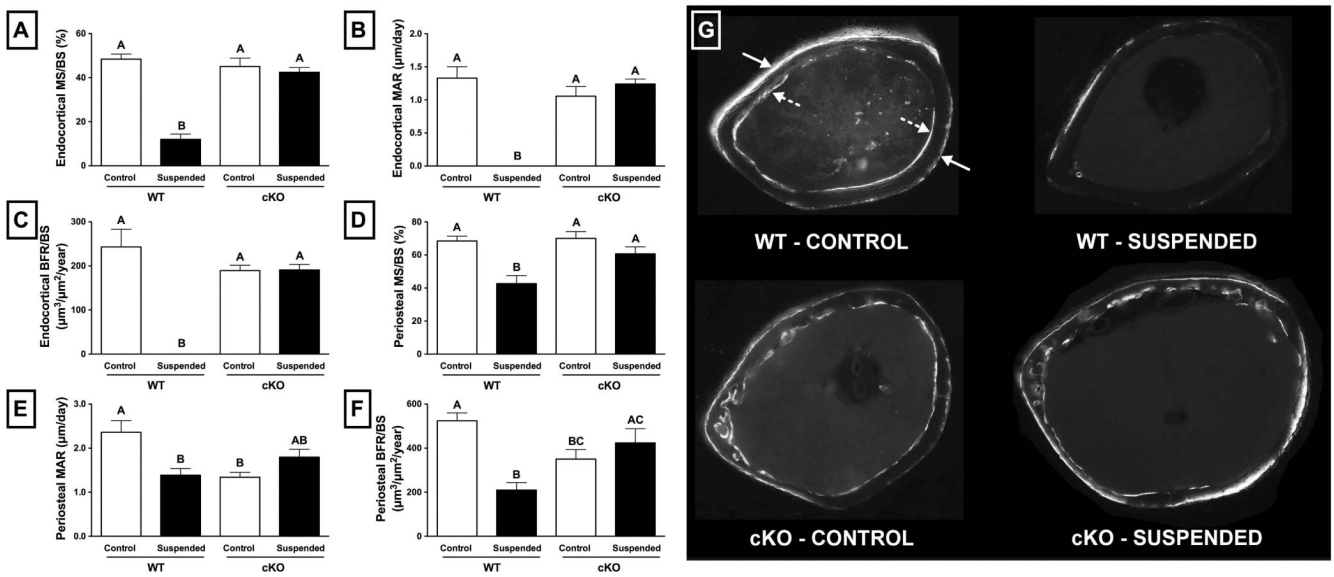

Figure 7.

Quantitative histomorphometry parameters for wild-type (WT) and Cx43 conditional knockout (cKO) mice following three weeks of normal loading (Control) or mechanical unloading via hindlimb suspension (Suspended). At the endocortical surface, (A) mineralizing surface normalized to bone surface (MS/BS) was significantly lower for WT mice subjected to unloading compared to control ($p<0.05$); however, this effect was not observed in cKO mice. (B) endocortical mineral apposition rate (MAR) and (C) endocortical bone formation rate normalized to bone surface (BFR/BS) were essentially obliterated with unloading in WT mice ($p<0.05$), and yet preserved in cKO. The periosteal surface experienced a similar attenuated suppression for cKO mice, although the magnitude was more modest. (D) Periosteal MS/BS, (E) periosteal MAR, and (F) periosteal BFR/BS. (G) Representative micrographs of femur sections used for quantification were taken under UV light at 4x magnification. The solid arrows indicate Calcein and alizarin red bone label incorporation at the periosteal surface, while the hatched arrows indicate label at the endocortical surface. Label incorporation is dramatically reduced in WT Suspended animals, and maintained in cKO Suspended. Comparisons via two-way ANOVA). Mean±SE. Different letters indicate significant difference, while similar letters indicate no difference.

Table 1

Summary of baseline trabecular bone parameters as assessed via microCT of wild-type (WT) and connexin 43 conditional knockout (cKO) mice (male, aged 6-months).

Parameter	WT	cKO
BV/TV (%)	16.24 ± 1.19	16.47 ± 1.29
Conn.D (1/mm^3)	70.39 ± 6.04	74.95 ± 7.86
Tb.Th (mm)	0.058 ± 0.001	0.061 ± 0.001
Tb.Sp (mm)	0.231 ± 0.008	0.234 ± 0.010
Tb.N (1/mm)	4.22 ± 0.12	4.16 ± 0.14
SMI (no units)	1.99 ± 0.11	2.15 ± 0.12
TMD (mg HA/cm^3)	239 ± 9	232 ± 11

Bone volume fraction (BV/TV); connectivity density (Conn.D); trabecular thickness (Tb.Th); trabecular separation (Tb.Sp), trabecular number (Tb.N), structure model index (SMI), trabeculartissue mineral density (TMD).

Data are presented as the mean±SE; n=25-30/group.

No significant difference observed for any parameter ($p>0.05$ via t-test).

Table 2

Summary of femur cortical morphological parameters as assessed via quantitative histomorphometry of wild-type (WT) and connexin 43 conditional knockout (cKO) mice (male, aged 6-months) under both control (normally loaded) and suspended (unloaded) conditions.

Parameter	WT		cKO	
	Control	Suspended	Control	Suspended
Tt.V (mm^3)	3.022 ± 0.092[a]	3.003 ± 0.089[a]	4.534 ± 0.180[b]	4.432 ± 0.131[b]
Ct.V (mm^3)	1.146 ± 0.052[a]	0.961 ± 0.015[a]	1.321 ± 0.089[b]	1.214 ± 0.062[b]
Ma.V (mm^3)	1.875 ± 0.076[a]	2.042 ± 0.093[a]	3.213 ± 0.121[b]	3.217 ± 0.138[b]
Ec.BS (mm^2)	5.196 ± 0.114[a]	5.378 ± 0.132[a]	6.834 ± 0.175[b]	6.725 ± 0.124[b]
Ps.BS (mm^2)	6.487 ± 0.085[a]	6.453 ± 0.092[a]	7.743 ± 0.156[b]	7.698 ± 0.107[b]

Total tissue volume (Tt.V), cortical bone volume (Ct.V), marrow cavity volume (Ma.V), endocortical bone surface (Ec.BS), periosteal bone surface (Ps.BS).

Data are presented as the mean±SE.

Different letters indicate significant difference ($p<0.05$ via two-way ANOVA), while the same letter indicates no difference.